AGU PUBLICATIONS

Geophysical Research Letters

RESEARCH LETTER
10.1002/2015GL065018

**Key Points:**
- Adjoint tomography reveals a deep slightly warmer (54 K to 127 K) mantle upwelling beneath Hangai
- Induced decompression melting generates partial melt that promotes heating of the lithosphere
- Thermally modified lithosphere isostatically supports Hangai Dome uplift at upper mantle depths

**Supporting Information:**
- Supporting Information S1
- Movie S1

**Correspondence to:**
M. Chen,
min.chen@rice.edu

**Citation:**
Chen, M., F. Niu, Q. Liu, and J. Tromp (2015), Mantle-driven uplift of Hangai Dome: New seismic constraints from adjoint tomography, *Geophys. Res. Lett.*, *42*, 6967–6974, doi:10.1002/2015GL065018.

Received 19 JUN 2015
Accepted 6 AUG 2015
Accepted article online 10 AUG 2015
Published online 3 SEP 2015



# Mantle-driven uplift of Hangai Dome: New seismic constraints from adjoint tomography

**Min Chen[1], Fenglin Niu[1,2], Qinya Liu[3], and Jeroen Tromp[4,5]**

[1]Department of Earth Science, Rice University, Houston, Texas, USA, [2]State Key Laboratory of Petroleum Resource and Prospecting and Unconventional Natural Gas Institute, China University of Petroleum, Beijing, China, [3]Department of Physics, University of Toronto, Toronto, Ontario, Canada, [4]Department of Geosciences, Princeton University, Princeton, New Jersey, USA, [5]Program in Applied and Computational Mathematics, Princeton University, Princeton, New Jersey, USA

**Abstract** The origin of Hangai Dome, an unusual large-scale, high-elevation low-relief landform in central Mongolia, remains enigmatic partly due to lack of constraints on its underlying seismic structure. Using adjoint tomography—a full waveform tomographic technique—and a large seismic waveform data set in East Asia, we discover beneath the dome a deep low shear wave speed (low-V) conduit indicating a slightly warmer (54 K to 127 K) upwelling from the transition zone. This upwelling is spatially linked to a broader uppermost mantle low-V region underlying the dome. Further observations of high compressional to shear wave speed ratios and positive radial anisotropy in the low-V region suggest partial melting and horizontal melt transport. We propose that the mantle upwelling induced decompression melting in the uppermost mantle and that excess heat associated with melt transport modified the lithosphere that isostatically compensates the surface uplift at upper mantle depths (>80 km).

## 1. Introduction

Topographically elevated more than 2 km above sea level, the intracontinental high-elevation low-relief Hangai Dome in central Mongolia bears an enigmatic origin (Figure 1). Initial calc-alkaline granitoids of the Hangai batholith possibly formed due to a Late Permian to Middle Triassic large magmatic event [*Donskaya et al.*, 2013]; this magmatic event is linked to northward subduction of the paleo-Mongol-Okhotsk ocean before its complete closure by the Early Cretaceous. Cenozoic alkaline volcanic basalt erupted sporadically in Mongolia since ~33 Ma, and the main Miocene volcanic rocks in the Hangai area are limburgites, analcime andesite-basalts, and trachy basalts [*Whitford-Stark*, 1987]. Post-12 Ma volcanic activity has been focused on the uplift of Hangai Dome [*Hunt et al.*, 2012].

Buoyancy due to mass deficit in both the lower crust/uppermost mantle and asthenosphere accounts for the "excess" topography of Hangai Dome [*Petit et al.*, 2002]. However, the mechanism producing such buoyancy remains a debated topic. Two end-member models invoke a mantle plume [*Khain*, 1990; *Windley and Allen*, 1993; *Cunningham*, 1998; *Barry et al.*, 2003; *Zorin et al.*, 2006; *Mordvinova et al.*, 2007, 2015; *Tiberi et al.*, 2008] or lithospheric processes [*Cunningham*, 2001; *Petit et al.*, 2002; *Barry et al.*, 2003; *Anderson*, 2005; *Hunt et al.*, 2012]. Mantle plume models suggest an active bottom-up process where a low-density mantle plume or asthenospheric diapir interacts with overlying lithosphere, possibly causing lithospheric thinning. Such models are qualitatively supported by observations of regionally elevated heat flow up to 120 mW/m$^2$ [*Tseesuren*, 2001], lithospheric thinning [*Zorin et al.*, 1990], rifting, and late Cenozoic alkaline volcanism [*Hunt et al.*, 2012]. Conversely, lithospheric models support a passive top-down process where convective removal of lithosphere due to preexisting thickening induces small-scale mantle upwelling of light asthenospheric material. A series of tomographic studies [*Koulakov*, 1998; *Villaseñor et al.*, 2001; *Friederich*, 2003; *Yanovskaya and Kozhevnikov*, 2003; *Lebedev et al.*, 2006; *Mordvinova et al.*, 2007, 2015; *Tiberi et al.*, 2008] have imaged a distinctive upper mantle low wave speed (low-V) anomaly beneath Hangai Dome and associated uplift in terms of a mantle plume or asthenospheric diapir. Due to differing classical tomographic techniques and data coverage, images of the low-V anomaly vary dramatically, and interpretations of the origin of the mantle upwelling are not conclusive. Geochemical evidence from Cenozoic alkaline basalts [*Barry et al.*, 2003] indicates that high heat flux plume-like thermal anomalies are not required, and instead melting of metasomatized lower lithosphere can be triggered by low-heat flux thermal anomalies. Because the origin

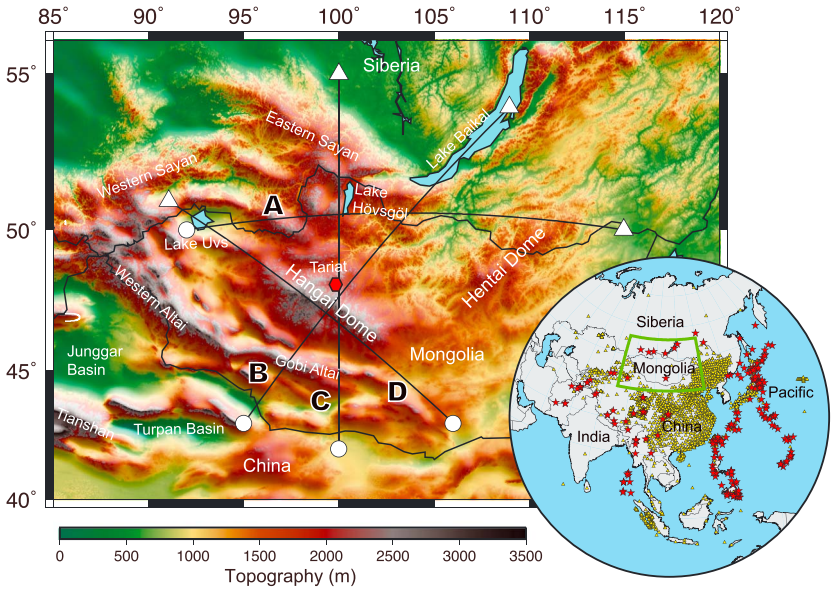


**Figure 1.** Topographic map of the Hangai-Hentai-Baikal area. Black lines indicate the four profiles marked by A–D, along which cross sections of seismic anomalies are shown in Figure 2. The inset shows the distribution of earthquakes (red stars) and stations (yellow triangles) used in this tomographic study.

of active mantle upwelling is ambiguous from previous tomographic studies, lithospheric processes are favored as the melting mechanism beneath Hangai Dome [*Hunt et al.*, 2012].

Detailed seismic imaging along a major transect crossing central Mongolia was carried out by the 2003 MOBAL (Mongolian-Baikal Lithosphere Seismological Transect) experiment, which revealed low-V upper mantle anomalies beneath Hangai Dome extending to transition zone depths [*Mordvinova et al.*, 2007, 2015; *Tiberi et al.*, 2008]. Our study presents an improved 3-D shear wave speed ($V_S$) model of the entire Mongolia area as well as models of two additional seismic properties indicative of temperature/partial melt and mantle flow direction, namely, (1) the isotropic compressional to shear wave speed ratio, $V_P/V_S$, and (2) the radial anisotropy parameter $\zeta = (V_{SH} - V_{SV})/V_S$, that is, the relative wave speed difference between horizontally traveling and horizontally (*SH*) and vertically (*SV*) polarized shear waves.

## 2. Data and Adjoint Tomography

Improvements in both full waveform tomography [*Tromp et al.*, 2005; *Fichtner et al.*, 2009; *Tape et al.*, 2009; *Zhu et al.*, 2012; *French and Romanowicz*, 2014] and seismic station coverage have enabled more detailed mapping of cold downwellings and hot upwellings in Earth's mantle. More specifically, adjoint tomography—a full waveform tomographic technique based on finite frequency theory and a spectral element method [*Komatitsch and Tromp*, 2002a, 2002b]—has recently been developed to render seismic images from large data sets [*Tromp et al.*, 2005; *Tape et al.*, 2009; *Zhu et al.*, 2012; *Chen et al.*, 2015]. The latest adjoint tomography study of East Asia [*Chen et al.*, 2015] (Texts S1 and S2 and Figures S1 to S3 in the supporting information) assimilates an unprecedented data set (Figure 1, inset) and reveals details of mantle anomalies, such as melts, subducting slabs, and fossil slabs due to subduction of the Pacific and other oceanic plates. While a previous paper [*Chen et al.*, 2015] covers the technical aspects of constructing the East Asia Radially Anisotropic Model (EARA2014), here we provide a more detailed interpretation of seismic wave speed features beneath Hangai Dome.

## 3. Results and Discussion

Cross sections through EARA2014 along four profiles in the Hangai-Hentai-Baikal area are shown in Figure 2. Two anomalous regions identified beneath Hangai Dome are denoted by LV1 and LV2 in Figure 2. Located at depths shallower than 150 km with a broad horizontal extent (~600 km to 800 km), LV1 is characterized by strong low $V_S$ ($< -3\,\%$) and a high $V_P/V_S$ ratio ($> 3\,\%$), indicating high temperatures and possible partial

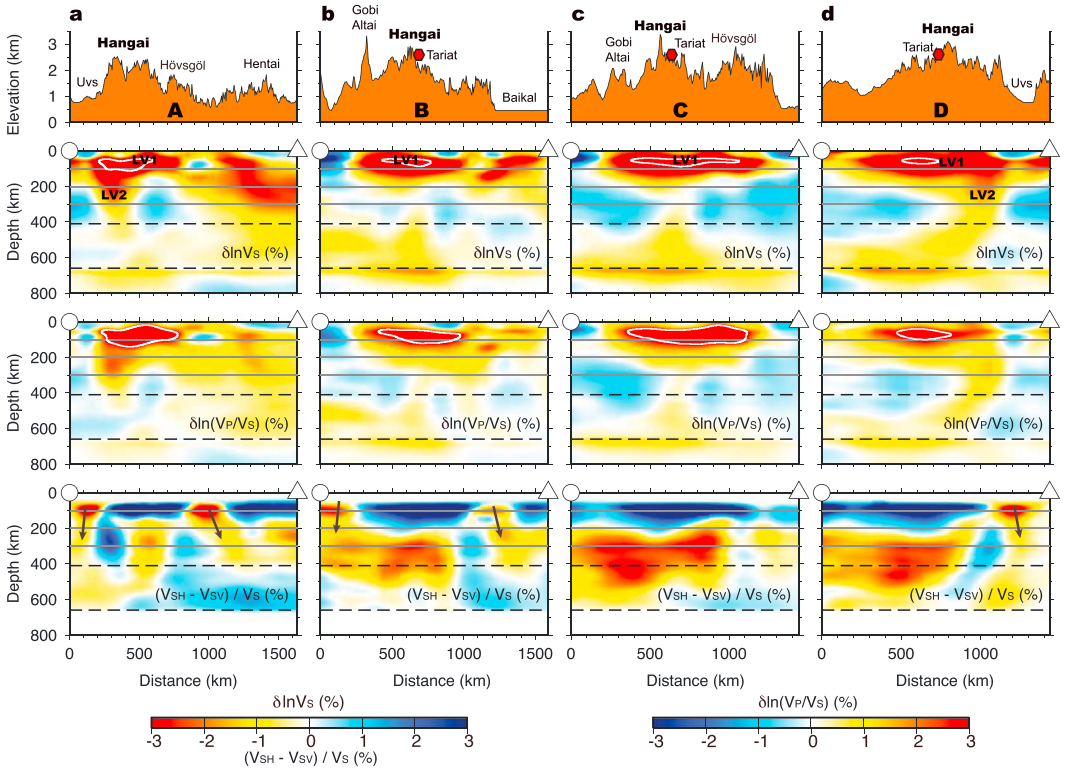


**Figure 2.** Cross sections showing surface elevations and seismic anomalies in the crust and upper mantle. (a–d) Cross sections along profiles A–D (indicated in Figure 1) are shown for (first row) surface elevation, (second row) relative shear wave speed anomalies $\delta lnV_S$, (third row) relative $V_P/V_S$ ratio anomalies $\delta ln(V_P/V_S)$, and (fourth row) radial anisotropy $(V_{SH} - V_{SV})/V_S$. White lines delineate − 6 % contours of $\delta lnV_S$ (Figure 2, second row) or 3 % contours of $\delta ln(V_P/V_S)$ (Figure 2, third row). Dashed lines represent the 410 km and 660 km discontinuities, and gray lines mark 100 km, 200 km, and 300 km depths. The low-V anomalies beneath Hangai Dome are marked by LV1 and LV2. Note that a thin wide low-Vs region that underlies the 660 could indicate unmodeled topography of the 660 discontinuity (Figures 2b–2d, second row). Black arrows indicate the interpreted downwelling location and direction from radial anisotropy (Figure 2, fourth row).

melting. Elevations in the Hangai area are clearly correlated with the thickness of LV1 (Figures 2 and S6 in the supporting information). Higher elevations are correlated with longer columns of LV1, such as those beneath the apex of Hangai Dome (Figures 2a–2c), while lower elevations correspond to shorter columns of LV1, such as those beneath Lake Uvs (Figures 2a and 2d) and the valley between Hangai Dome and Hentai Dome (Figure 2a). On the contrary, high $V_S$ and low $V_P/V_S$ ratios indicate cold temperatures and absence of melt, such as those beneath the region south of the Gobi Altai (Figures 2b and 2c). Moreover, LV1 exhibits strongly positive radial anisotropy (up to 5%) ($V_{SH} > V_{SV}$) (Figures 2, S4, and S5 and Text S3 in the supporting information), consistent with a previous surface wave study [*Villaseñor et al.*, 2001]. In the same depth range of LV1 along its edges, strongly negative radial anisotropy is found beneath relatively low elevations, such as Lake Uvs, indicating possible downwelling of relatively cold and denser mantle material, which corresponds to less negative Bouguer anomalies (~ − 50 mGal) compared to Hangai Dome, where there are strongly negative Bouguer anomalies (~ − 150 mGal) (Figures S5d and S6b). At a depth of ~ 150 km, LV1 appears to be connected to a narrow conduit LV2 (~200 km to 400 km wide) beneath the northwestern part of Hangai Dome. LV2 is characterized by moderately low $V_S$ (1% to 2% reductions) and moderately high $V_P/V_S$ ratios (1% to 2% increases) above the transition zone (Figure 2a). As LV2 dips downward to the southeast and spans across the mantle transition zone right beneath central Hangai (Figure 2d), $V_S$ becomes weakly low and the $V_P/V_S$ ratio weakly high (Figures 2b–2d).

The narrow conduit LV2 (Figures 2 and 3 and Movie S1 in the supporting information) beneath northwestern Hangai is consistent with previous observations from the 2003 MOBAL experiment [*Tiberi et al.*, 2008; *Mordvinova et al.*, 2015]. This feature is confirmed to be robust, because it still emerges if the inversion starts

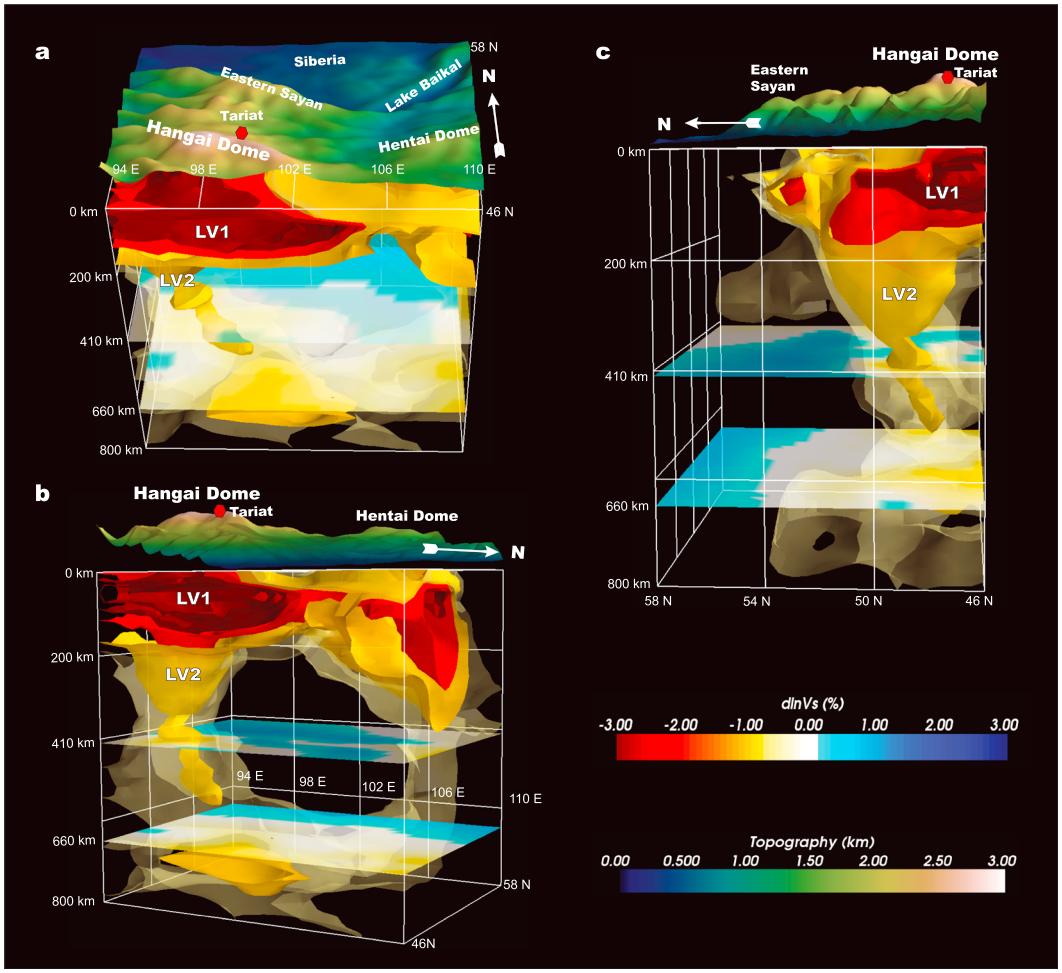


**Figure 3.** Three-dimensional visualization of the low shear wave speed (low-V) structure beneath the Hangai region rendered from EARA2014 [*Chen et al.*, 2015]. (a) Isosurfaces of low-V anomalies viewed downward from the south, (b) viewed upward from the southeast, and (c) viewed from the east. Isosurfaces of low-V anomalies, in percent referenced to the regional mean at each depth, are plotted from −4% to −1% with 1% intervals. The −0.5% isosurface is also plotted in semitransparent light yellow. Maps of shear wave speed anomalies are shown at 410 km and 660 km depths. Surface topography with vertical exaggeration is superimposed for reference.

with a 1-D initial model in the depth range from 100 km to 300 km [*Chen et al.*, 2015]. Additional resolution tests also prove that our data coverage and imaging technique can resolve such features at depths of ~300 km (Figures S1 and S2). Another wider conduit (Figures 2a and 3b) beneath the Hentai-Baikal area has moderately low $V_S$ and weakly high $V_P/V_S$ ratios extending into the mantle transition zone. These two conduits appear to originate in the same low-V region residing in the lower transition zone or even as deep as about 800 km (isosurface at −0.5% in Figure 3 and Movie S1 in the supporting information), but they feed two separate shallower low-V regions (<150 km) beneath Hangai Dome (LV1) and Hentai Dome. The relatively more anomalous LV1 region (Figures S4 to S6) might explain the higher topography, higher heat flow [*Dorofeeva and Lysak*, 2010], more abundant Cenozoic volcanism [*Barry et al.*, 2003], and more negative Bouguer gravity anomalies [*Petit et al.*, 2002] observed at Hangai Dome compared to Hentai Dome.

Our tomographic images indicate that the LV2 conduit extends down to about 800 km (Figure 3). Receiver function analysis of the 410 km and 660 km discontinuities beneath central Hangai (in the vicinity of station HD25 of network XL) reveals a mantle transition zone ~10–20 km thinner than the global average (~250 km) (Text S4 and Figures S9 and S10 in the supporting information), suggesting a slightly warmer thermal anomaly spanning across the mantle transition zone which coincides with the location of LV2 (Figure S11 in the supporting information). At 410 km depth, given a pressure-depth gradient of ~38 MPa km$^{-1}$

[*Dziewonski and Anderson*, 1981] and Clapeyron slopes of 1.5 MPa $K^{-1}$ to 3.5 MPa $K^{-1}$ for the $\alpha$-olivine to $\beta$-spinel phase change [*Akaog and Ito*, 1993; *Bina and Helffrich*, 1994], a 5 km topographic depression on the 440 discontinuity implies a weakly high-temperature anomaly of 54 K to 127 K. At 660 km depth, given a pressure-depth gradient of ~40 MPa $km^{-1}$ [*Dziewonski and Anderson*, 1981] and Clapeyron slopes of −3.0 MPa $K^{-1}$ to −2.1 MPa $K^{-1}$ for the $\gamma$-spinel to perovskite + magnesiowüstite phase change [*Akaog and Ito*, 1993; *Bina and Helffrich*, 1994], a 5 km topographic uplift on the 660 discontinuity also implies a weakly high-temperature anomaly of 67 K to 95 K. Using the tomographic shear wave speed anomaly and a value of −1.0% per 100 K at 410 km depth and −0.65% per 100 K at 660 km depth, determined by [*Karato*, 1993, Figure 1a] to relate shear wave speed and temperature, we infer a 0.6% to 1.27% $V_S$ reduction at 410 and a 0.44% to 0.62% $V_S$ reduction at 660, similar to the ~0.5% to 1% $V_S$ reduction we observe (Figure 3). In conclusion, a ~0.5% to 1% $V_S$ reduction as imaged here and ~10 km of TZ thinning are consistent with a low-heat thermal anomaly (54 K to 127 K warmer) in the transition zone.

Global tomographic models do not contain low-V anomalies above the core-mantle boundary beneath the Hangai area [*Bijwaard et al.*, 1998; *Kustowski et al.*, 2008; *Ritsema et al.*, 2011; *French and Romanowicz*, 2014]. Cenozoic basalts are small in volume, erupted sporadically over ~30 Myr, and are low-degree melts with a mid-ocean ridge basalt (MORB)-like isotopic signature. Combined seismological and geochemical evidence suggests that LV2 does not originate from the base of the mantle. Instead, lower mantle low-V anomalies appear to depths of only ~1500 km, right above a high-speed anomaly in the depth range of 1500 km to 2500 km [*Bijwaard et al.*, 1998], which has been interpreted as subducted Mongol-Okhotsk lithosphere [*van der Voo et al.*, 1999]. Since Cenozoic volcanism in the Hangai area is more recent (in the past 12 Myr) and Mongol-Okhotsk subduction stopped at ~150 Ma, LV2 is not likely associated with Jurassic Mongol-Okhotsk subduction. Because we do not know the residence time of the Mongol-Okhotsk slab inside the transition zone before it sank into the lower mantle, we cannot completely rule out the possibility of initial volcanism at ~33 Ma being related to the paleo-Mongol-Okhotsk slab. However, based on broader East Asia tomographic images [*Chen et al.*, 2015, Figures 7 and 9], there is no discernable high-V slab feature indicating a relic Mongol-Okhotsk slab inside or immediately below the mantle transition zone. Therefore, we favor a connection between post-12 Ma Hangai volcanism and the presently subducting Pacific slab. The formation of LV2 may be due to hot fertilized peridotite detaching from stagnant Pacific slab as it sinks into the lower mantle [*Zorin et al.*, 2006], although slab edge-driven return flow may provide an alternative explanation [*Faccenna et al.*, 2010].

Our observation of LV1 (Figures 2 and 3) possibly indicates an anomalous lithosphere thermally modified by heat associated with partial melting and melt transport. About 6% $V_S$ reductions (Figure 2), 3 % high $V_P/V_S$ ratio anomalies (Figure 2), and even more reduced $V_{SV}$ (less than 4.2 km/s) (Figures S4 and S5) exist between depths of ~50 km (around the Moho) and ~90 km. These observations imply the presence of about 2–3% partial melt in the lower crust and uppermost mantle [*Takei*, 2000], consistent with a steeper geotherm at the Moho derived from xenoliths in the Tariat region (central Hangai) [*Ionov et al.*, 1998]. The focused mantle upwelling LV2 revealed beneath northwestern Hangai may have provided asthenospheric melt as the initial source at Tariat, although a detailed melt migration path is unresolved by our study. Furthermore, basalts in the Hangai area are less depleted and very different in terms of isotopic composition compared to xenoliths [*Stosch et al.*, 1986; *Ionov et al.*, 1994]. Isotopic evidence suggests two main source components of Hangai magma [*Barry et al.*, 2003]: (1) those similar to Indian-MORB indicating a shallow asthenospheric source instead of a lithospheric mantle contribution and (2) those similar to EM1-type basalts suggesting possible contamination from fluids/sediments subducted during the long subduction history of the Western Pacific slab, which is common for Cenozoic basaltic magmas all across East Asia. The mantle upwelling possibly generated early magma due to decompression melting and subsequently triggered melting of volatile-enriched lithospheric mantle beneath Hangai Dome to form LV1 at shallower depths [*Barry et al.*, 2003; *Hunt et al.*, 2012] (Figure 4). Because LV1 spatially corresponds to positive radial anisotropy, indicating horizontal mantle flow, we speculate that partial melt near the Moho beneath the dome may have migrated horizontally (Figure 4).

Contributions to uplift of Hangai Dome may include crustal thickening, a crustal and upper mantle mass deficit, and/or basal traction caused by dynamic mantle convection. Geodetic modeling suggests no significant neotectonic deformation at Hangai Dome due to the remote India-Asia collision [*Liu and Bird*, 2008]. Therefore, tectonic-driven crustal shortening at Hangai Dome may be insignificant. A viable mechanism for

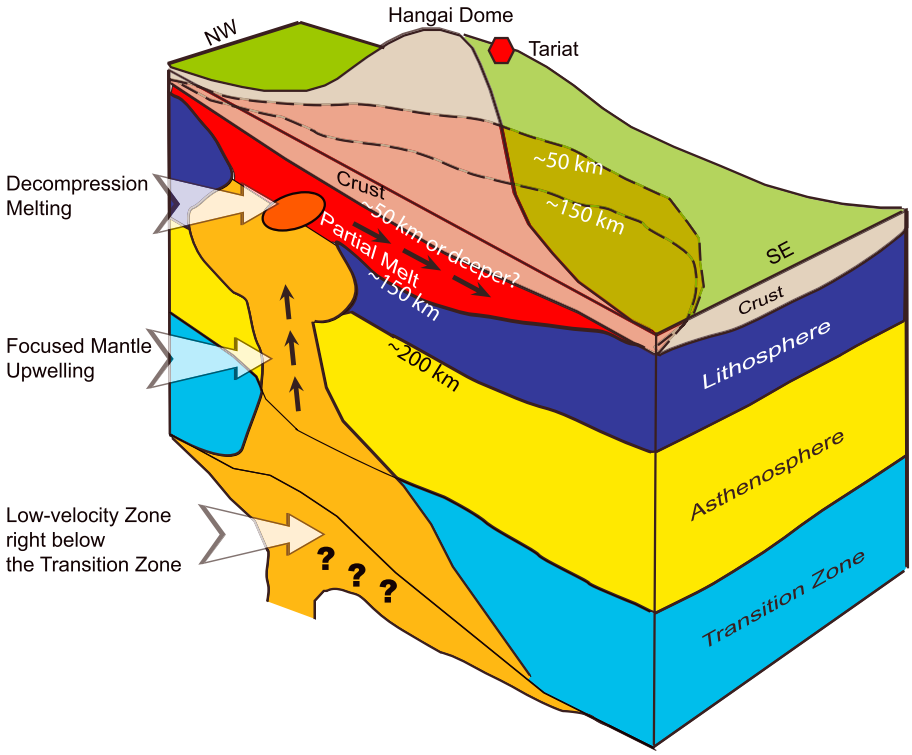


**Figure 4.** Schematic interpretation of the origin of uplift of Hangai Dome.

crustal thickening could be magmatic underplating [*McKenzie*, 1984]. Airy type isostatic adjustment requires addition of ~11 km to 22 km thick underplated basalt (Text S3 in the supporting information). Post-12 Ma basalts at Hangai are erupted sporadically in small volume and with low-degree melt. This limited surface expression of an underlying magma supply makes the presence of a thick underplated basalt layer unlikely. Further investigations of underplating require high-resolution seismic imaging of Moho depth variations and crustal and uppermost mantle wave speeds using a regional dense seismic array, such as the temporary Incorporated Research Institutions for Seismology (IRIS)/Portable Array Seismic Studies of the Continental Lithosphere (PASSCAL) array with 75 stations deployed at Hangai Dome. On the other hand, our seismic constraints on crustal and mantle structure cannot distinguish dynamic topography due to basal traction from isostatically compensated topography, unless we have very robust constraints on the density-wave speed relation and crustal thickness [*Molnar et al.*, 2015]. Given that density and shear wave speed perturbations are positively correlated at least in the upper mantle [*Anderson*, 1987; *Karato*, 1993], the ~600 km to 800 km wide LV1 may represent a lighter lithosphere, thereby accounting for the observed long-wavelength (~600 km to 800 km) negative (~100 mGal to 250 mGal) Bouguer gravity anomaly (Text S3 and Figure S6 in the supporting information). Further analysis of model EARA2014 indicates that the lithosphere can isostatically support surface uplift of Hangai Dome with a compensation depth of ~ 80 km or even greater (up to 150 km) based on Pratt isostasy (Text S3 and Figures S7 and S8 in the supporting information). This makes the mass deficit in this depth range consistent with that inferred from gravity modeling (100 km to 200 km) [*Petit et al.*, 2002] and much deeper than the maximum estimated depth of the crust (57 km) from a receiver function study [*Stachnik et al.*, 2014].

## 4. Conclusions

Our tomographic model of Hangai Dome suggests that a slightly warmer (54 K to 127 K) thermal anomaly—possibly originating from above the underlying flat slab in the transition zone—feeds lighter asthenospheric material through a localized (~200 km to 400 km wide) area at the bottom of the lithosphere. Large-scale convective removal of the lithosphere at its bottom is not observed. Our model favors an active bottom-up asthenospheric upwelling with low-heat influx. Infiltrated asthenospheric material generates partial melt through decompression melting during ascent. Horizontal melt transport at shallower depths promotes

heating of lithosphere and thermally modified lithosphere in a wide region (~600 km to 800 km across). Further analysis of EARA2014 shear wave speed anomalies favors an isostatic contribution of Hangai surface uplift from lithospheric depths of at least 80 km, which exceeds the maximum possible Moho depths [*Stachnik et al*., 2014] and suggests an additional contribution to isostatic support from an upper mantle mass deficit.

Future work should focus on identifying a possible underplated basalt layer at the bottom of the crust and/or dynamic topography by obtaining a more accurate map of the Moho, characterizing the crustal and upper mantle density distribution, and numerical modeling of dynamic topography based on seismic tomographic images.

**Acknowledgments**

We thank the Editor (Michael Wysession), Reviewer 1 (anonymous), and Reviewer 2 (James Ni) for their constructive and insightful comments that helped improve the manuscript. We also thank Cin-Ty Lee and Richard Carlson for their helpful suggestions to strengthen the interpretation of our results. This research was supported by NSF grants 1063057, 1112906, 1345096, and ACI-1053575 and NSERC grants 487237 and 490919. We thank the various networks that contributed data (F-net, CEArray, NECESSArray, INDEPTH IV Array, IRIS/IDA, and other regional and global seismic networks), as well as the Rice Research Computing Support Group. The majority of waveform data were provided by the China Seismic Array Data Management Center at the Institute of Geophysics, China Earthquake Administration. The open source spectral-element software package SPECFEM3D_GLOBE, the seismic measurement software package FLEXWIN, and the moment-tensor inversion package CMT3D used for this article are freely available for download via the Computational Infrastructure for Geodynamics (CIG; geodynamics.org).

The Editor thanks James Ni and an anonymous reviewer for their assistance in evaluating this paper.

## References

Akaog, M., and E. Ito (1993), Refinement of enthalpy measurement of MgSiO3 perovskite and negative pressure-temperature slopes for perovskite-forming reactions, *Geophys. Res. Lett.*, *20*(17), 1839–1842, doi:10.1029/93GL01265.

Anderson, D. L. (1987), A seismic equation of state II. Shear properties and thermodynamics of the lower mantle, *Phys. Earth Planet. Inter.*, *45*, 307–323.

Anderson, D. L. (2005), Large igneous provinces, delamination, and fertile mantle, *Elements*, *1*(5), 271–275, doi:10.2113/gselements.1.5.271.

Barry, T. L., A. D. Saunders, P. D. Kempton, B. F. Windley, M. S. Pringle, D. Dorjnamjaa, and S. Saandar (2003), Petrogenesis of Cenozoic basalts from Mongolia: Evidence for the role of asthenospheric versus metasomatized lithospheric mantle sources, *J. Petrol.*, *44*(1), 55–91.

Bijwaard, H., W. Spakman, and E. R. Engdahl (1998), Closing the gap between regional and global travel time tomography, *J. Geophys. Res.*, *103*(B12), 30,055–30,078, doi:10.1029/98JB02467.

Bina, C. R., and G. Helffrich (1994), Phase transition Clapeyron slopes and transition zone seismic discontinuity topography, *J. Geophys. Res.*, *99*(B8), 15,853–15,860, doi:10.1029/94JB00462.

Chen, M., F. Niu, Q. Liu, J. Tromp, and X. Zhen (2015), Multiparameter adjoint tomography of the crust and upper mantle beneath East Asia: 1. Model construction and comparisons, *J. Geophys. Res. Solid Earth*, *120*, doi:10.1002/2014JB011638.

Cunningham, W. D. (1998), Lithospheric controls on late Cenozoic construction of the Mongolian Altai, *Tectonics*, *17*(6), 891–902, doi:10.1029/1998TC900001.

Cunningham, W. D. (2001), Cenozoic normal faulting and regional doming in the southern Hangay region, Central Mongolia: Implications for the origin of the Baikal rift province, *Tectonophysics*, *331*, 389–411, doi:10.1016/S0040-1951(00)00228-6.

Donskaya, T. V., D. P. Gladkochub, A. M. Mazukabzov, and A. V. Ivanov (2013), Late Paleozoic – Mesozoic subduction-related magmatism at the southern margin of the Siberian continent and the 150 million-year history of the Mongol-Okhotsk Ocean, *J. Asian Earth Sci.*, *62*, 79–97, doi:10.1016/j.jseaes.2012.07.023.

Dorofeeva, R. P., and S. V. Lysak (2010), Heat flow of central Asia *Proceedings World Geothermal Congress*, Bali, Indonesia.

Dziewonski, A. M., and D. L. Anderson (1981), Preliminary reference Earth model, *Phys. Earth Planet. Inter.*, *25*(4), 297–356, doi:10.1016/0031-9201(81)90046-7.

Faccenna, C., T. W. Becker, S. Lallemand, Y. Lagabrielle, F. Funiciello, and C. Piromallo (2010), Subduction-triggered magmatic pulses: A new class of plumes?, *Earth Planet. Sci. Lett.*, *299*, 54–68, doi:10.1016/j.epsl.2010.08.012.

Fichtner, A., B. L. N. Kennett, H. Igel, and H.-P. Bunge (2009), Full seismic waveform tomography for upper-mantle structure in the Australasian region using adjoint methods, *Geophys. J. Int.*, *179*(3), 1703–1725, doi:10.1111/j.1365-246X.2009.04368.x.

French, S. W., and B. A. Romanowicz (2014), Whole-mantle radially anisotropic shear velocity structure from spectral-element waveform tomography, *Geophys. J. Int.*, *199*, 1303–1327, doi:10.1093/gji/ggu334.

Friederich, W. (2003), The S-velocity structure of the East Asian mantle from inversion of shear and surface waveforms, *Geophys. J. Int.*, *153*, 88–102.

Hunt, A. C., I. J. Parkinson, N. B. W. Harris, T. L. Barry, N. W. Rogers, and M. Yondon (2012), Cenozoic volcanism on the Hangai Dome, Central Mongolia: Geochemical evidence for changing melt sources and implications for mechanisms of melting, *J. Petrol.*, *53*(9), 1913–1942, doi:10.1093/petrology/egs038.

Ionov, D. A., A. W. Hofmann, and N. Shimizu (1994), Metasomatism-induced melting in mantle xenoliths from Mongolia, *J. Petrol.*, *35*(3), 753–785, doi:10.1093/petrology/35.3.753.

Ionov, D. A., S. Y. O'Reilly, and W. L. Griffin (1998), A geotherm and lithospheric cross-section for central Mongolia, in *Mantle Dynamics and Plate Interactions in East Asia*, *Geodynamics Ser.*, vol. 27, edited by M. Flower et al., pp. 127–153, AGU, Washington, D. C.

Karato, S. (1993), Importance of anelasticity in the interpretation of seismic tomography, *Geophys. Res. Lett.*, *20*(15), 1623–1626, doi:10.1029/93GL01767.

Khain, V. E. (1990), Origin of the central Asian mountain belt: Collision or mantle diapirism, *J. Geodyn.*, *11*, 389–394.

Komatitsch, D., and J. Tromp (2002a), Spectral-element simulations of global seismic wave propagation—I. Validation, *Geophys. J. Int.*, *149*, 390–412, doi:10.1046/j.1365-246X.2002.01653.x.

Komatitsch, D., and J. Tromp (2002b), Spectral-element simulations of global seismic wave propagation—II. Three-dimensional models, oceans, rotation and self-gravitation, *Geophys. J. Int.*, *150*, 303–318, doi:10.1046/j.1365-246X.2002.01716.x.

Koulakov, I. (1998), Three-dimensional seismic structure of the upper mantle beneath the central part of the Eurasian continent, *Geophys. J. Int.*, *133*, 467–489, doi:10.1046/j.1365-246X.1998.00480.x.

Kustowski, B., G. Ekström, and A. M. Dziewoński (2008), Anisotropic shear-wave velocity structure of the Earth's mantle: A global model, *J. Geophys. Res.*, *113*, B06306, doi:10.1029/2007JB005169.

Lebedev, S., T. Meier, and R. D. van der Hilst (2006), Asthenospheric flow and origin of volcanism in the Baikal Rift area, *Earth Planet. Sci. Lett.*, *249*, 415–424, doi:10.1016/j.epsl.2006.07.007.

Liu, Z., and P. Bird (2008), Kinematic modelling of neotectonics in the Persia-Tibet-Burma orogen, *Geophys. J. Int.*, *172*(2), 779–797, doi:10.1111/j.1365-246X.2007.03640.x.

McKenzie, D. (1984), A possible mechanism for epeirogenic uplift, *Nature*, *307*(5952), 616–618, doi:10.1038/307616a0.

Molnar, P., P. C. England, and C. H. Jones (2015), Mantle dynamics, isostasy, and the support of high terrain, *J. Geophys. Res. Solid Earth*, *120*, 1932–1957, doi:10.1002/2014JB011724.

Mordvinova, V. V., A. Deschamps, T. Dugarmaa, J. Deverchére, M. Ulziibat, V. A. Sankov, A. A. Artem'ev, and J. Perrot (2007), Velocity structure of the lithosphere on the 2003 Mongolian-Baikal transect from SV waves, *Izvestiya, Phys. Solid Earth*, *43*(2), 119–129, doi:10.1134/S1069351307020036.

Mordvinova, V. V., A. V. Treussov, and E. K. Turutanov (2015), Nature of the mantle plume under Hangai (Mongolia) based on seismic and gravimetric data, *Dokl. Earth Sci.*, *460*(1), 92–95, doi:10.1134/S1028334X15010201.

Petit, C., J. De, and D. Fairhead (2002), Deep structure and mechanical behavior of the lithosphere in the Hangai-Hövsgöl region, Mongolia: New constraints from gravity modeling, *Earth Planet. Sci. Lett.*, *197*, 133–149.

Ritsema, J., A. Deuss, H. J. Van Heijst, and J. H. Woodhouse (2011), S40RTS: A degree-40 shear-velocity model for the mantle from new Rayleigh wave dispersion, teleseismic traveltime and normal-mode splitting function measurements, *Geophys. J. Int.*, *184*(3), 1223–1236, doi:10.1111/j.1365-246X.2010.04884.x.

Stachnik, J., A. Meltzer, S. Souza, and R. Russo (2014), Crustal and upper mantle structure of the Hangay Dome, central Mongolia, *2014 IRIS Workshop Abstract*.

Stosch, H.-G., G. W. Lugmair, and V. I. Kovalenko (1986), Spinel peridotite xenoliths from the Tariat Depression, Mongolia. II: Geochemistry and Nd and Sr isotopic composition and their implications for the evolution of the subcontinental lithosphere, *Geochim. Cosmochim. Acta*, *50*, 2601–2614.

Takei, Y. (2000), Acoustic properties of partially molten media studied on a simple binary system with a controllable dihedral angle, *J. Geophys. Res.*, *105*(B7), 16,665–16,682, doi:10.1029/2000JB900124.

Tape, C., Q. Liu, A. Maggi, and J. Tromp (2009), Adjoint tomography of the southern California crust, *Science*, *325*, 988–992, doi:10.1126/science.1175298.

Tiberi, C., A. Deschamps, J. Déverchère, C. Petit, J. Perrot, D. Appriou, V. Mordvinova, T. Dugaarma, M. Ulzibaat, and A. A. Artemiev (2008), Asthenospheric imprints on the lithosphere in Central Mongolia and Southern Siberia from a joint inversion of gravity and seismology (MOBAL experiment), *Geophys. J. Int.*, *175*(3), 1283–1297, doi:10.1111/j.1365-246X.2008.03947.x.

Tromp, J., C. Tape, and Q. Liu (2005), Seismic tomography, adjoint methods, time reversal and banana-doughnut kernels, *Geophys. J. Int.*, *160*(1), 195–216, doi:10.1111/j.1365-246X.2004.02453.x.

Tseesuren, B. (2001), Geothermal resources in Mongolia and potential uses, *Rep. 15, Geotherm. Training Program. United Nations Univ.*, 347–374.

Van der Voo, R., W. Spakman, and H. Bijwaard (1999), Mesozoic subducted slabs under Siberia, *Nature*, *397*, 246–249.

Villaseñor, A., M. H. Ritzwoller, A. L. Levshin, M. P. Barmin, E. R. Engdahl, W. Spakman, and J. Trampert (2001), Shear velocity structure of central Eurasia from inversion of surface wave velocities, *Phys. Earth Planet. Inter.*, *123*, 169–184, doi:10.1016/S0031-9201(00)00208-9.

Whitford-Stark, J. L. (1987), A survey of Cenozoic volcanism on mainland Asia, *Geol. Soc. Am. Spec. Pap.*, *213*, 1–74, doi:10.1130/SPE213-p1.

Windley, B. F., and M. B. Allen (1993), Mongolian plateau: Evidence for a late Cenozoic mantle plume under central Asia, *Geology*, (21), 295–298, doi:10.1130/0091-7613(1993)021<0295.

Yanovskaya, T. B., and V. M. Kozhevnikov (2003), 3D *S*-wave velocity pattern in the upper mantle beneath the continent of Asia from Rayleigh wave data, *Phys. Earth Planet. Inter.*, *138*, 263–278, doi:10.1016/S0031-9201(03)00154-7.

Zhu, H., E. Bozdağ, D. Peter, and J. Tromp (2012), Structure of the European upper mantle revealed by adjoint tomography, *Nat. Geosci.*, *5*(7), 493–498, doi:10.1038/ngeo1501.

Zorin, Y. A., M. R. Novoselova, E. K. Turutanov, and V. M. Kozhevnikov (1990), Structure of the lithosphere of the Mongolian-Siberian mountainous province, *J. Geodyn.*, *11*, 327–342.

Zorin, Y. A., E. K. Turutanov, V. M. Kozhevnikov, S. V. Rasskazov, and A. I. Ivanov (2006), The nature of Cenozoic upper mantle plumes in East Siberia (Russia) and Central Mongolia, *Russ. Geol. Geophys.*, *47*(10), 1056–1070.